



UNIVERSITY OF LEEDS

This is a repository copy of *Oxidation kinetic analysis of diesel particulate matter using single- and multi-stage methods*.

White Rose Research Online URL for this paper:
<http://eprints.whiterose.ac.uk/147677/>

Version: Accepted Version

Article:

Gao, J, Chen, H, Tian, G et al. (2 more authors) (2019) Oxidation kinetic analysis of diesel particulate matter using single- and multi-stage methods. *Energy & Fuels*, 33 (7). pp. 6809-6816. ISSN 0887-0624

<https://doi.org/10.1021/acs.energyfuels.9b01297>

© 2019 American Chemical Society. This document is the Accepted Manuscript version of a Published Work that appeared in final form in *Energy & Fuels*, copyright © American Chemical Society after peer review and technical editing by the publisher. To access the final edited and published work see <https://doi.org/10.1021/acs.energyfuels.9b01297>.
Uploaded in accordance with the publisher's self-archiving policy.

Reuse

Items deposited in White Rose Research Online are protected by copyright, with all rights reserved unless indicated otherwise. They may be downloaded and/or printed for private study, or other acts as permitted by national copyright laws. The publisher or other rights holders may allow further reproduction and re-use of the full text version. This is indicated by the licence information on the White Rose Research Online record for the item.

Takedown

If you consider content in White Rose Research Online to be in breach of UK law, please notify us by emailing eprints@whiterose.ac.uk including the URL of the record and the reason for the withdrawal request.



eprints@whiterose.ac.uk
<https://eprints.whiterose.ac.uk/>

Oxidation kinetic analysis of diesel particulate matter using single- and multi-stage methods

Jianbing Gao, Haibo Chen, Guohong Tian, Chaochen Ma, and Fei Zhu

Energy Fuels, **Just Accepted Manuscript** • DOI: 10.1021/acs.energyfuels.9b01297 • Publication Date (Web): 16 Jun 2019

Downloaded from <http://pubs.acs.org> on June 24, 2019

Just Accepted

“Just Accepted” manuscripts have been peer-reviewed and accepted for publication. They are posted online prior to technical editing, formatting for publication and author proofing. The American Chemical Society provides “Just Accepted” as a service to the research community to expedite the dissemination of scientific material as soon as possible after acceptance. “Just Accepted” manuscripts appear in full in PDF format accompanied by an HTML abstract. “Just Accepted” manuscripts have been fully peer reviewed, but should not be considered the official version of record. They are citable by the Digital Object Identifier (DOI®). “Just Accepted” is an optional service offered to authors. Therefore, the “Just Accepted” Web site may not include all articles that will be published in the journal. After a manuscript is technically edited and formatted, it will be removed from the “Just Accepted” Web site and published as an ASAP article. Note that technical editing may introduce minor changes to the manuscript text and/or graphics which could affect content, and all legal disclaimers and ethical guidelines that apply to the journal pertain. ACS cannot be held responsible for errors or consequences arising from the use of information contained in these “Just Accepted” manuscripts.

Oxidation kinetic analysis of diesel particulate matter using single- and multi-stage methods

Jianbing Gao,^{*,†,‡} Haibo Chen,[†] Guohong Tian,[§] Chaochen Ma,[‡] Fei Zhu,[‡]

[†] Institute for Transport Studies, University of Leeds, Leeds LS2 9JT, UK

[‡] School of Mechanical Engineering, Beijing Institute of Technology, Beijing 100081, China

[§] Department of Mechanical Engineering Sciences, University of Surrey, Guildford GU2 7XH, UK

* Corresponding author:

Chaochen Ma

E-mail: machaochen1900@163.com

School of Mechanical Engineering, Beijing Institute of Technology, Beijing 100081, China

Jianbing Gao

E-mail: redonggaojianbing@163.com

Institute for Transport Studies, University of Leeds, Leeds LS2 9JT, UK

1
2
3
4 **Abstract:** Plenty of diesel particulate matter (PM) is emitted into the atmosphere in the forms of
5 raw PM and partially oxidized PM. Comprehensive investigations of PM oxidation behavior and
6 kinetics contribute to lower PM emission and optimize the PM capture device design. In this paper,
7 diesel PM oxidation behavior was investigated using different temperature control programs, then,
8 the oxidation kinetics were analyzed using Arrhenius equation. Nanostructure, Fourier Transform
9 Infrared Spectroscopy (FTIR) and Raman characteristics were adopted to further clarify PM
10 oxidation kinetics. The results indicated that PM oxidation showed multi-stage reactions, and
11 reaction rate decreased rapidly in the isothermal process, with activation energy increasing. Heat
12 transfer limitation significantly decreased the activation energy, also affected the following
13 reactions. In the narrow temperature range 523°C~537°C, the activation energy of partially oxidized
14 and aging PM was smaller than the values of the initial oxidation stage. The oxidation
15 transformation phase had a huge potential of evolving into the heat transfer limitations. The
16 activation energy of partially oxidized and aging PM was smaller than the value of raw PM at the
17 end of oxidation, which was caused by the catalytic reaction of metal ash. Diesel PM nanostructure
18 changed from the onion like to core-shell like structures after partial oxidation.

19
20
21
22
23
24
25
26
27
28
29
30
31
32
33 **Keywords:** Diesel particulate matter; oxidation behaviors; oxidation kinetics; activation energy;
34 nanostructure

35 36 37 **1. Introduction**

38 Particulate matter suspending in the atmosphere has caused serious problems to human health and
39 environment ¹, especially at urban areas. The towers used for removing suspending particles in the
40 air had been established in Xi'an of China, and a significant decrease of particle concentration was
41 observed around the towers. It is a more effective approach of preventing the PM from emitting into
42 the atmosphere to alleviate the issues caused by particles. PM from diesel engines makes a great
43 contribution to the suspending particles. Sharma ² from Massachusetts Institute of Technology
44 (MIT) designed a professional device to capture diesel PM, and the captured PM was used to create
45 air-ink for artists, which actually was to recycle air pollutant to make art. Nevertheless, diesel
46 particulate filter (DPF) ³ is the most successful product to decrease PM emission in commercial
47 field. What's more, DPF regeneration problem must be resolved to decrease the fuel penalty caused
48 by the increase of engine backpressure ⁴. Post fuel injection is commonly used to achieve DPF
49 regeneration, with the results of diesel PM being partially oxidized. Due to the increase of specific
50
51
52
53
54
55
56
57
58
59
60

1
2
3
4 surface area and pore size after partial oxidation ⁵, it is easier to absorb organic compound (OC)
5
6 when it is exposed into the atmosphere. PM oxidation behaviors and oxidation kinetics are vital to
7
8 resolve DPF regeneration problems and optimizing the design. In addition, such researches
9
10 contribute to decrease the PM emission from diesel engines, and lay the foundation of reducing PM
11
12 in the atmosphere.

13
14 The commonly used method to test PM oxidation behaviors is thermogravimetric analysis (TGA),
15
16 which monitors the sample mass changes at a given temperature program ^{6, 7}. Based on the
17
18 oxidation profiles, different methods were used to calculate kinetic parameters (activation energy,
19
20 pre-exponential factors, and reaction rate constant) ⁷⁻⁹. Activation energy of diesel PM sampled at
21
22 different conditions (engine operation conditions, engine types, fuel types, aftertreatment
23
24 technologies) was in the range of 80 kJ/mol ~230 kJ/mol ¹⁰⁻¹⁷. The values, calculated using multiple
25
26 ramp rate oxidation profiles (Kissinger, Akahira and Sunose method), increased generally with
27
28 mass drop in the oxidation process. López-Fonseca et al. ⁷ obtained the oxidation kinetic lines using
29
30 single-step oxidation profiles, with results that the temperature ramp rates (1.5 °C/min~7.5 °C/min)
31
32 had a limited effect on activation energy. Due to the disadvantages of TGA method as mentioned in
33
34 reference ⁹, Gao et al. ¹¹ put forward a differential scanning calorimetry (DSC) based method to
35
36 investigate PM oxidation behaviors and calculate the oxidation kinetic parameters. This method ¹¹
37
38 accurately showed the mass loss history caused by the chemical reactions rather than OC
39
40 volatilization.

41
42 PM oxidation behaviors presented closely related to physico-chemical properties which greatly
43
44 depended on PM formation conditions ¹⁸⁻²¹. PM formed at high engine load conditions tended to
45
46 contain less OC which could be divided into high volatilization OC and low volatilization OC,
47
48 whose temperature ranges were 50 °C~200 °C and 200 °C~450 °C, respectively ²². Biodiesel PM
49
50 was considered to be easier to oxidize than diesel PM because of higher oxygen content. In the
51
52 oxidation process, the oxygen content decreased greatly when mass loss was more than 40% for
53
54 biodiesel PM, while it was ~20% for diesel PM ²³. Oxygen containing functional groups provided
55
56 active sites for PM oxidation, and FTIR was used to detect the functional groups contained in PM ²⁴,
57
58 ²⁵.

59
60 PM oxidation activity is also partly dependent on nanostructure which generally were the onion and
core-shell like structures. Additionally, it is widely accepted that the oxidative activity of diesel PM

1
2
3
4 with onion like structures were more active than that of core-shell like structures ¹⁵. During the
5 oxidation, the nanostructure experienced the onion like structures, core-shell like structures, then
6 densely arranged bands ²⁶. Song et al. ²⁷ hold the opinion that nanostructure had a smaller effect on
7 PM oxidation behaviors than oxygen containing functional groups. It was demonstrated by the fact
8 that the oxidation rate of biodiesel PM was five times higher than that of diesel PM although
9 biodiesel PM nanostructure was more orderly arranged. High resolution transmission electronic
10 microscopy (HRTEM) was an effective approach to observe the PM nanostructure ²⁸. It is a
11 milestone that nanostructure evolutions of individual PM during oxidation were observed directly²⁹,
12 which provided a strong foundation of PM oxidation modeling. Raman spectra contain vibration
13 and rotation information of molecules, further the crystallite disorder degree and graphitization
14 could be analyzed, which showed strong relations with PM oxidation behaviors ^{30,31}.

15
16
17
18
19
20
21
22
23
24
25 The oxidation kinetic changes in the oxidation process have been researched based on single-stage
26 in many references ^{7, 32, 33}, nevertheless, detailed analysis of multi-stage oxidation of diesel PM was
27 limited. In addition, details of the oxidation kinetics in the oxidation process were neglected if
28 multiple ramp rate method was applied to calculate the kinetic lines ¹². In the oxidation process,
29 heat transfer limitation happened when much heat was released, which caused rapid mass drop. The
30 apparent oxidation kinetic parameters and oxidation behaviors would be distorted when heat
31 transfer limitation happened ^{11, 34}, so that the heat transfer limitation was tried to avoid in researches.
32 As indicated in reference ³⁴, double peaks were observed in soot oxidation if heat transfer limitation
33 happened that the first one was attributed to a thermal runaway reaction. The detailed characteristics
34 of the TGA profiles changed with the experiment conditions ³⁵, such as sample mass, temperature
35 ramp rate, oxygen content and carrier gas flow rate. However, to the authors' knowledge, no
36 reference was available to date the influence of the heat transfer limitation on normal oxidation
37 reactions, also the effect of heat transfer limitation on apparent activation energy was seldom
38 analyzed.

39
40
41
42
43
44
45
46
47
48
49
50
51
52 In this paper, detailed analysis of PM oxidation behaviors and oxidation kinetics were conducted in
53 the multi-stage oxidation process (stage temperature control program) and single-stage oxidation
54 process. Activation energy in the oxidation process was calculated using oxidation profiles and
55 Arrhenius equation. The influence of heat transfer limitation on the normal stage of oxidation and
56 activation energy was firstly analyzed. Then, the nanostructure, FTIR and Raman characteristics
57
58
59
60

were researched to further clarify the oxidation behaviors and oxidation kinetics.

2. Experimental section

2.1 The test engine

The tested engine was the power of a small generator which was widely used in construction sites, environmental sanitation and agricultural industries. The detailed specifications of the engine were shown in reference ³⁶. The diesel engine was used less than 100 h, and the properties of the diesel fuel are listed in Table 1. The engine speed was a constant value (3000 r/min) because the output voltage of the generator was unchangeable (220 V). The engine load was adjusted by the electric power output of the generator.

Table 1 Properties of diesel fuel

Properties	Value
Viscosity (20 °C)	4.1 mm ² /s
Density	850 kg/m ³
Cetane number	52
S content	0.0042%
H/C ratio	0.156
50% distillation points	290 °C
95% distillation points	340 °C

2.2 Instruments used in the experiments

Oxidation profiles of diesel PM were obtained at given conditions using a TGA device (DTG-60) that was made by Shimadzu. The detailed specifications of the TGA device were shown in reference ¹¹. The nanostructure of diesel PM was obtained by transmission electron microscope (JEM-2100), and the magnifications were set as 40, 000× and 500, 000×. Low magnification HRTEM figures were used for the statistics of primary particle diameter distributions. Before the nanostructure test, suspensions were created by ultrasonication of PM within acetone. One drop of the suspension was deposited on a lacey C/Cu TEM grid, then, the TEM grid was dried under accent light to volatilize acetone. The functional groups of diesel PM were tested using a FTIR device (Shimadzu IRAffinity-1s), the wave scope of FTIR spectrum was 500 cm⁻¹~4000 cm⁻¹. An Invia Raman device with an Ar-ion laser source (633 nm) was used to obtain the PM Raman spectra

1
2
3
4 which contain the vibration and rotation information of the molecules, further to analyse the
5 molecular structures. The first order Raman shift was in the range of $700\text{ cm}^{-1}\sim 2000\text{ cm}^{-1}$. Double
6 peaks were observed generally in the first order Raman spectra, and their Raman shifts were
7 corresponding to 1350 cm^{-1} (D peak) and 1590 cm^{-1} (G peak), respectively.
8
9

10 11 **2.3 Diesel PM collections and preparations**

12
13 In this paper, three kinds of diesel PM samples, namely raw PM, partially oxidized PM and aging
14 PM, were used to conduct the experiments. Raw PM was collected at 80% engine load conditions,
15 without any pre-treatment before test, and the distance between the exhaust valves and sampling
16 position was $\sim 2.0\text{ m}$, where the exhaust temperature was $203\text{ }^{\circ}\text{C}$. It was collected using a self-made
17 PM sampling filter, which was made of metal net. The metal net was pre-treated under oxygen and
18 high temperature atmosphere, and the exhaust was undiluted. The raw PM was peeled off from
19 metal net and was sealed stored at non-oxygen atmosphere as soon as PM was collected. In order to
20 obtain the partially oxidized PM, raw PM was pre-treated at high temperature and air atmosphere.
21 The pre-treatment process was as the following: raw PM was heated at $5\text{ }^{\circ}\text{C}/\text{min}$ from room
22 temperature (carrier gas: air) using TGA device, until 40% mass loss; then the air was switched as
23 N_2 , and the sample was cooled to ambient temperature. In the whole process, the air and N_2 flow
24 rate was $100\text{ mL}/\text{min}$. Aging PM was obtained by exposing partially oxidized PM in air for 40 days
25 to imitate the aging process (aging PM).
26
27
28
29
30
31
32
33
34
35
36
37

38 39 **2.4 TGA experiment conditions**

40
41 In this paper, two temperature control programs were used to conduct TGA experiments. (a) Raw
42 PM was heated at $5\text{ }^{\circ}\text{C}/\text{min}$ from room temperature to $650\text{ }^{\circ}\text{C}$ in air atmosphere ($100\text{ mL}/\text{min}$). In
43 the process, it was kept at isothermal conditions for 15 min at three points $200\text{ }^{\circ}\text{C}$, $450\text{ }^{\circ}\text{C}$ and
44 $550\text{ }^{\circ}\text{C}$. The multi-stage temperature program was used to simulate the multi-stage reaction process.
45 The initial mass of raw PM in the process was 3 mg. (b) All the three kinds of PM samples were
46 heated from room temperature to $700\text{ }^{\circ}\text{C}$ at $5\text{ }^{\circ}\text{C}/\text{min}$ in air ($100\text{ mL}/\text{min}$), then, cooling to room
47 temperature. The initial mass was $\sim 4\text{ mg}$ for raw PM, while it was $\sim 3\text{ mg}$ for partially oxidized PM
48 and aging PM.
49
50
51
52
53
54
55

56 57 **3. Oxidation kinetics parameter extraction**

58 Calculation of oxidation kinetic parameters is based on the Arrhenius equation format, as shown in
59 Equation 1,
60

$$-\frac{dm}{dt} = km^n p_{O_2}^r = A \exp\left(-\frac{E}{RT}\right) m^n p_{O_2}^r \quad (1)$$

Where m , t , k , n , p_{O_2} , r , A , E , R , T are sample mass, time, reaction rate constant, reaction order for carbon, partial pressure of oxygen, reaction order for oxygen, pre-exponential factor, activation energy, the universal gas constant (8.314 J/mol·K) and temperature. It is known that the surface area and pore size of the carbonaceous samples increased during oxidation³⁷. However, any changes in the surface area and pore size were not considered in the simplified kinetic expression. References^{38,39} showed that the reaction orders were close to unit that the values of n and r were 1. So that Equation 1 was transferred to Equation 2,

$$\ln\left(-\frac{dm}{m \cdot dt}\right) = \ln(A p_{O_2}) - \frac{E}{RT} \quad (2)$$

In a small temperature range, $\ln(-dm/(m \cdot dt))$ shows a linear correlation with $-/(R \cdot T)$. E and A can be calculated from the slope and intercept form Equation 2. In the whole oxidation process, the slopes and intercepts changed gradually due to the changes of physico-chemical properties^{11, 15}. PM surface area and pore size increased, also the catalytic reactions of ash enhanced during the oxidation process, however, oxygen containing functional groups decreased and graphitization were aggravated. The activation energy changes in the oxidation process depended on the joint actions of these factors^{15, 40}. Known from the reference⁷, the single ramp rate method was adopted to obtain the oxidation kinetic lines, which demonstrated that the temperature ramp rate almost had no effect on apparent activation energy.

4. Results and discussion

In this part, the research was divided into two sections. Firstly, the oxidation behaviors and oxidation kinetics in the single- and multi-stage oxidation processes were researched, also the heat transfer limitation was analyzed; Then, PM nanostructure, FTIR and Raman characteristics were investigated to further clarify PM oxidation behaviors.

4.1 Oxidation behavior and kinetic analysis

PM oxidation profiles showed closely related to temperature histories and PM ingredients which were dependent on many factors, such as engine types^{12, 22}, fuel types^{33, 41}, engine operation conditions^{11, 42}, exhaust gas recirculation (EGR)⁴³ and sampling conditions¹⁴. In TGA experiments, mass loss below 200 °C was caused by the oxidation and volatilization of high volatile OC, and it was low volatile OC in the range of 200 °C~450 °C. Soot oxidation dominated the mass loss when

the temperature was above 450 °C.

Figure 1(a) shows multi-stage oxidation profiles of raw PM under multi-stage temperature control program. The mass dropped slightly when temperature was lower than 450 °C, which was explained by the fact that a small amount of OC (low volatility and high volatility) was contained in raw PM due to high sampling temperature. Nevertheless, the mass loss was obvious when temperature was higher than 450 °C, where reaction rate increased with temperature in an exponential manner⁴⁴. The 200 °C isothermal stage was a transition phase where the reaction transferred from high volatility OC to low volatility OC. However, oxidation hardly happened in this stage, which was verified in the reference¹¹, where DSC method was used to test the heat release in oxidation process. The oxidation rate increased significantly in the end of the second stage (200 °C~450 °C); In the region of temperature higher than 450 °C, the mass loss percentage almost linearly increased with temperature. Mass loss rate decreased evidently when it was in the 550 °C isothermal conditions compared with that of temperature-rise period (around 550 °C). In the isothermal conditions, graphitization was aggravated and oxygen content decreased, also the crystallites were more orderly arranged, which caused the oxidation activity to decrease²⁶. The oxidation rate was recovered gradually once the isothermal condition was interrupted.

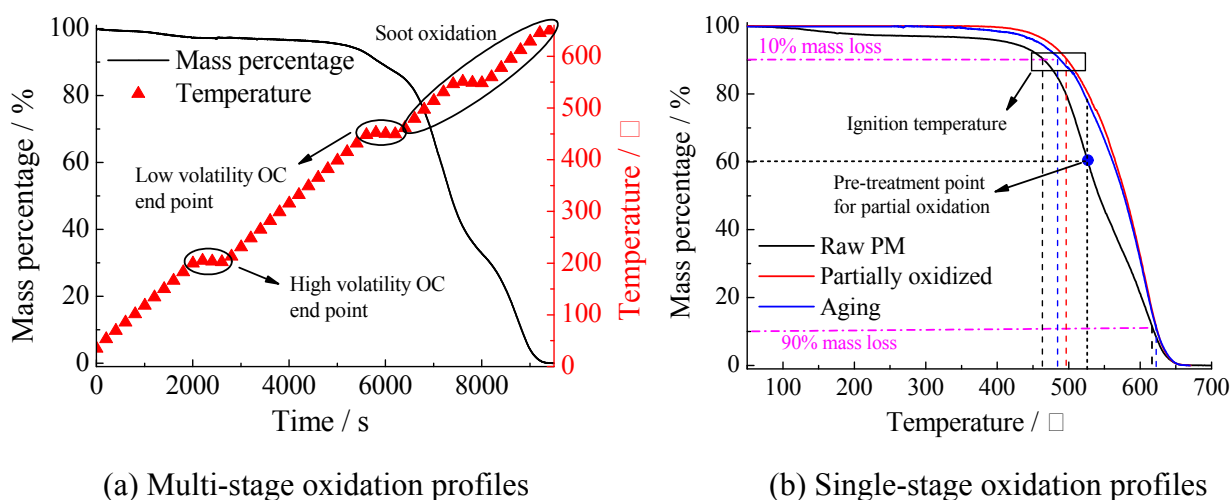


Figure 1 TGA profiles under different temperature control programs

Figure 1(b) shows the oxidation profiles at the single-stage oxidation process. The pre-treatment temperature of partially oxidized PM in Section 2.3 was ~530 °C which was around the isothermal conditions (550 °C) in Figure 1(a). Sample mass began to drop ~450 °C for partially oxidized PM, where OC oxidation was almost finished. The ignition temperature of partially oxidized PM was

~20 °C higher than raw PM. In addition, the value decreased slightly after aging in air, however, it was still higher than raw PM, as indicated in Figure 1(b). The burn out temperatures were almost the same for these three kinds of PM samples, which implied that the pre-treatment had a limited effect on oxidation behaviors of high temperatures.

The activation energy changes in the oxidation process can be clearly shown in the oxidation kinetic lines which were obtained using Equation 1 and oxidation profiles. Figure 2 shows the oxidation kinetic curves under multi-stage temperature program. The slopes of the kinetic curves in Figure 2 were activation energy. The calculated activation energy was anamorphic when temperature was low, since OC volatilization dominated mass loss, which had been demonstrated in reference ¹¹. Mass loss was weak when temperature was lower than 400 °C, which led to serious fluctuations of differential mass loss. The influence of ambient conditions (vibrations and noise) on oxidation kinetic lines was more conspicuous if the mass loss rate was slow. The activation energy was almost the same before and after the second isothermal stage (450 °C), however, it increased after the third isothermal stage (550 °C). It was indicated that high temperature conditions (e.g. 550 °C) significantly decreased the oxidation activity, nevertheless, it was limited for low temperature pre-treatment (lower than 450 °C).

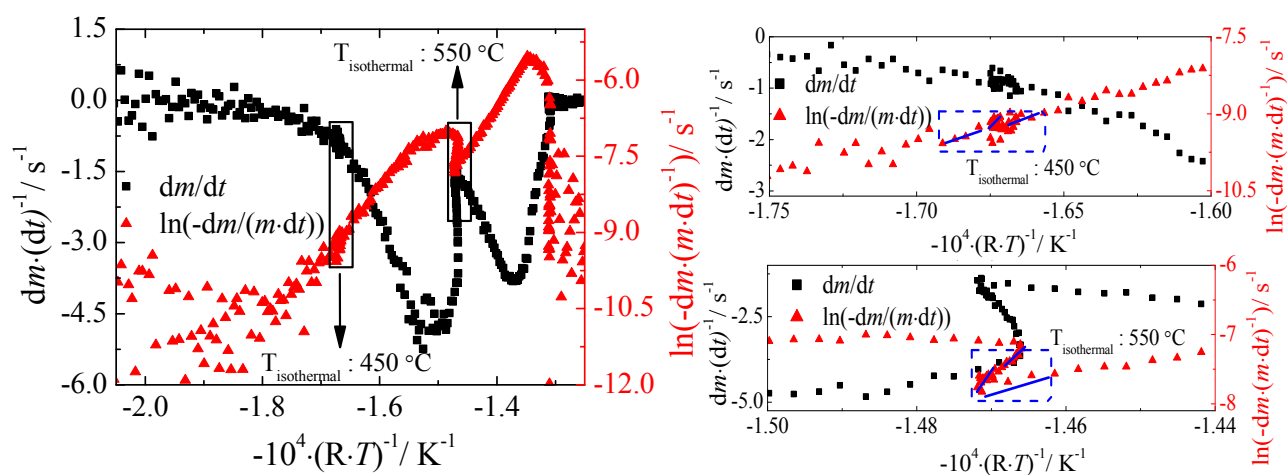
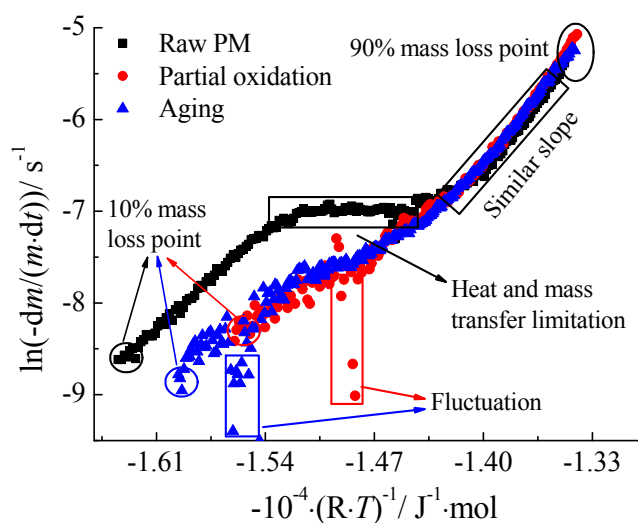


Figure 2 Oxidation kinetic curves under multi-stage temperature program

Figure 3 shows the oxidation kinetic curves of the three PM samples in the single-stage temperature program, they covered the mass loss percentage range of 10%~90%. In the oxidation process, there was an abnormal phase for raw PM, where the apparent activation energy was much lower than conventional values, which was caused by the heat transfer limitation. Heat transfer limitation often happened around the point of maximum mass loss rate, where much heat was released, with the

1
2
3
4 results of rapid temperature increase in PM. The temperature of PM interior was much higher than
5 the controlled value (apparent temperature) if heat transfer limitation happened, which caused
6 higher reaction rate constant and faster oxidation, with the results of the second peak in differential
7 thermogravimetric (DTG) curves, as indicated in Figure 4. There were several points being
8 seriously deviated from the kinetic curves (fluctuations), as cycled in the Figure 4, which was
9 caused by the ambient effect (vibrations and noise) that led to the sudden changes in DTG curves.
10 The slopes of the three kinetic curves were similar when the temperature was in the range of
11 592 °C~619 °C.
12
13
14
15
16
17
18
19



20
21
22
23
24
25
26
27
28
29
30
31
32
33
34
35
36
37
38
39
40
41
42
43
44
45
46
47
48
49
50
51
52
53
54
55
56
57
58
59
60
Figure 3 Oxidation kinetic curves in the single-stage temperature program

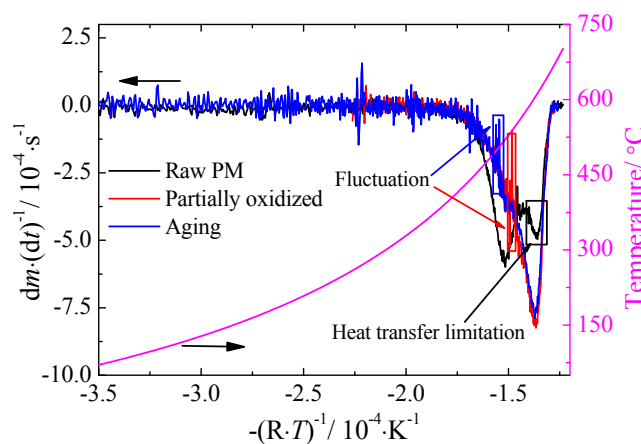


Figure 4 Differential thermogravimetric curves

The apparent activation energy of the three PM samples in the oxidation process is listed in Table 2. The activation energy during the oxidation process increased generally with oxidation temperature⁸, which was different from the results in the paper. Because the Kissinger–Akahira–Sunose (KAS) method⁸ was used to calculate the activation energy that the activation energy was discontinuous,

which led to the missing of detailed information at some points. Partial oxidation and aging in air had a limited influence on activation energy at the positions, where the oxidation temperature was higher than pre-treatment temperature (i.e. 450 °C in this paper). Activation energy of the partially oxidized PM and aging PM was slightly lower than raw PM samples in the range of 592°C~619 °C, which was caused by more serious catalytic reactions for partially oxidized PM and aging PM. Because both the two samples were pre-treated at high temperature which caused higher ash content compared with raw PM. It was demonstrated that metals in ash presented evident catalytic actions on PM oxidation^{45, 46}, with the clear results that Ca, Mg and Zn had high catalytic actions on soot oxidation, while Na showed an excellent performance on hydroxide reaction. For raw diesel PM, heat transfer limitation led to much heat release in the temperature range of 518 °C~556 °C, with the results that the apparent activation energy (10.8 kJ·mol⁻¹) was much lower than normal values in other temperature regions (470~518 °C and 592 ~619 °C). The heat transfer limitation also brought about an effect on the activation energy (96.4 kJ·mol⁻¹) in the following reactions (556 °C~592 °C) that the value was still smaller than the normal ones.

Table 2 Apparent activation energy of PM samples in the oxidation process (single-stage temperature program)

Samples	Activation energy/ kJ·mol ⁻¹ (temperature range/ °C)			
Raw PM	147.5 (470~518)	10.8 (518~556)	96.4 (556~592)	211.7 (592~619)
Partially oxidized	123.7 (495~537)	93.5(525~537)	210.8 (537~557)	196.4 (557~623)
Aging	120.5 (480~523)	87.0 (523~548)	205.4 (548~622)	

For the partially oxidized PM, the activation energy increased gradually, then, decreased slightly at the end of the oxidation process, which was consistent with López-Fonseca's⁸ investigation. It was caused by more severe catalytic actions of ash. The activation energy changes at the end of the oxidation process were also affected by graphitization that the joint effect dominated the activation energy changes. Another phenomenon was also observed that the activation energy dropped evidently in a narrow temperature range (~530 °C) for both partially oxidized and aging PM. It should be noted that the start point of the heat transfer limitation in raw PM was also around 530 °C. The potential relations of the heat transfer limitation and its temperature range will be explored in future work. In the process of aging in air, some organic compounds were adhered to PM surface so

that it caused slightly decrease of ignition temperature and activation energy compared with partially oxidized PM.

4.2 PM nanostructure, FTIR and Raman characteristics

Figure 5 shows the nanostructure of the three PM samples. In low resolution TEM figures, diesel PM presented the branch-like structures with many particles overlapped. Obviously, the primary particle diameters decreased after partial oxidation, meanwhile, aging in air had a small effect on the diameter distributions, as shown in Figure 6. The particle size distribution was the statistical results of more than 300 particles from low resolution TEM figures. The diameter corresponding to the peaks shifted to a smaller value for partially oxidized and aging PM compared with raw PM. All the particles were smaller than 100 nm for partially oxidized and aging PM. This statistical approach used for the primary diameter distributions was completely different from the professional methods, such as electrical low-pressure impactor (ELPI) and engine exhaust particle sizer (EEPS), scanning mobility particle sizer (SMPS) and condensation particle counter (CPC)⁴⁷⁻⁵⁰. In this paper, the diameter was the geometry value, nevertheless, it was aerodynamic diameter for those tested using professional instruments^{13, 51, 52}.

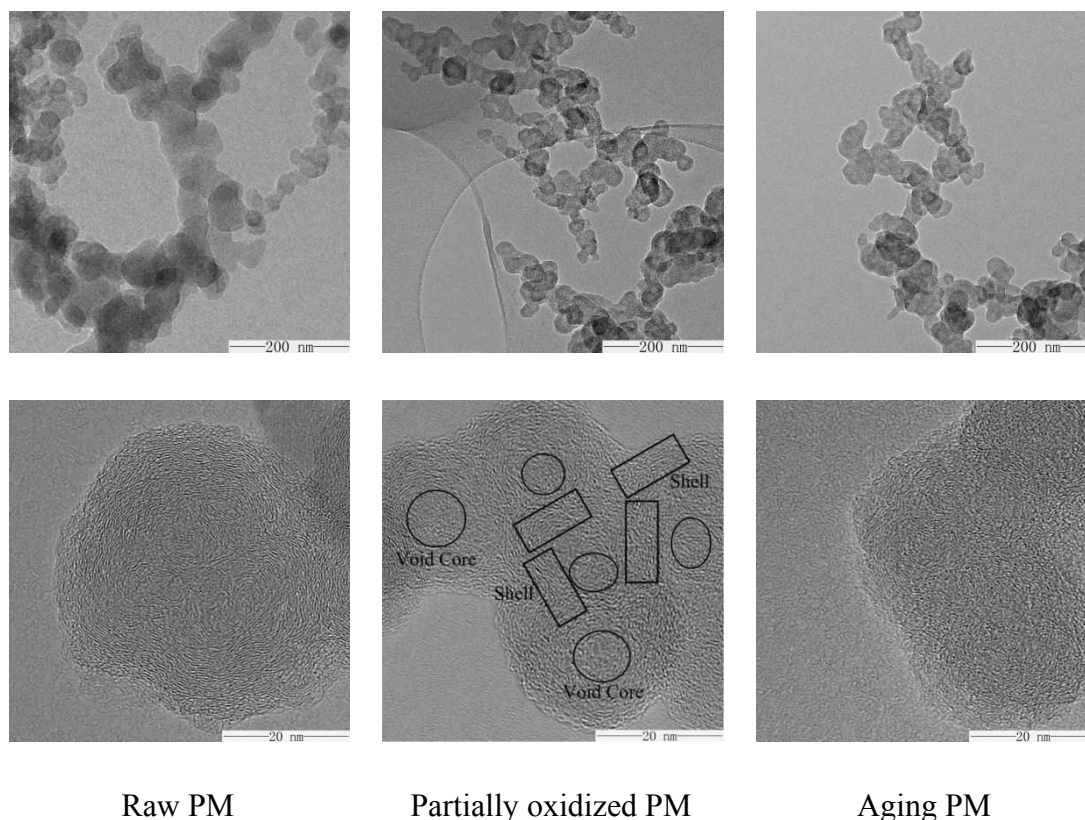


Figure 5 Nanostructure of different PM samples

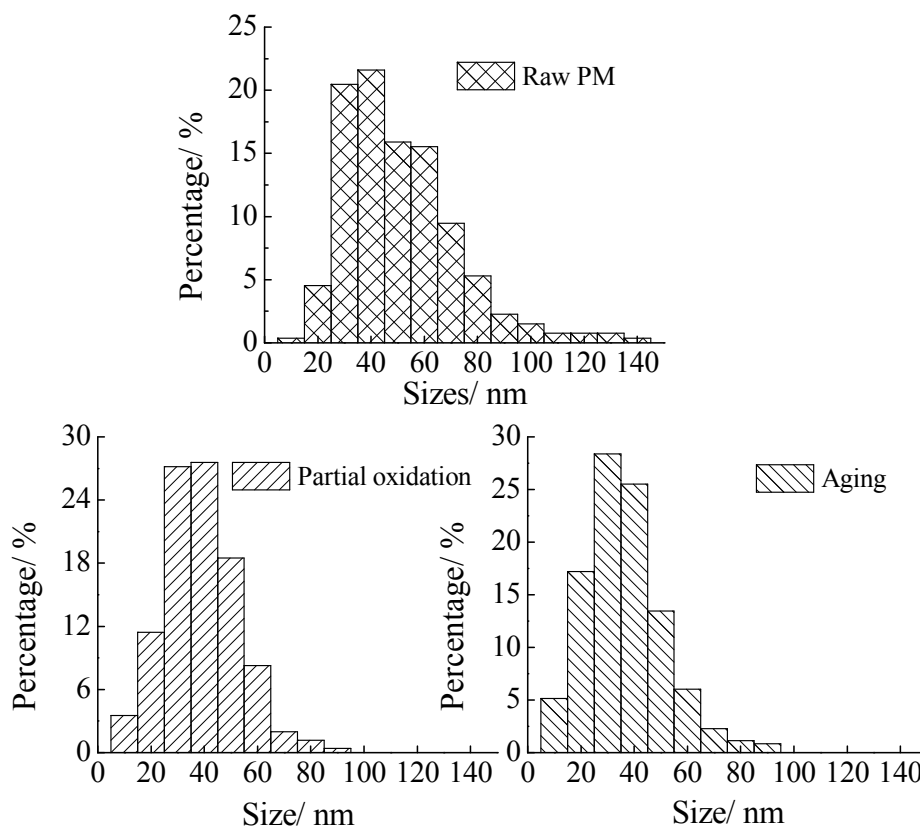


Figure 6 Primary particle size of diesel PM

In the high resolution TEM figures, primary particles showed the onion like and core-shell like structures, which were greatly dependent on the in-cylinder combustions^{26, 41, 53}. After partial oxidation, nanostructure was transformed from onion like structures to core-shell like structures with void cores and smaller diameters. Surface oxidation happened firstly due to large amounts of active sites on the surfaces, and their easier access to oxygen. Meanwhile, surface oxidation activity decreased gradually because of the drop of active sites. Then, oxidation was transferred from the surfaces into inner cores whose oxidation activity was still high. The inner cores contained oxygen-containing OC which provided active sites. This led to the activation energy drop ~ 530 °C for partially oxidized and aging PM, as mentioned above, this stage was named as transformation stage. Oxidation transferring from the outer surfaces into inner cores aggravated the chemical reactions with much more heat release in a short time, which was speculated as the origin of heat transfer limitation for raw PM in this paper. If under the conditions of huge sample mass, this caused PM oxidation to be out of control in a short time, further, the mass loss rate increased. Conclusions from the above, the transformation stage lasted only a short time in normal oxidation, and it presented the potentials of evolving into the reactions with heat transfer limitation. The

oxidation model was shown in Figure 7.

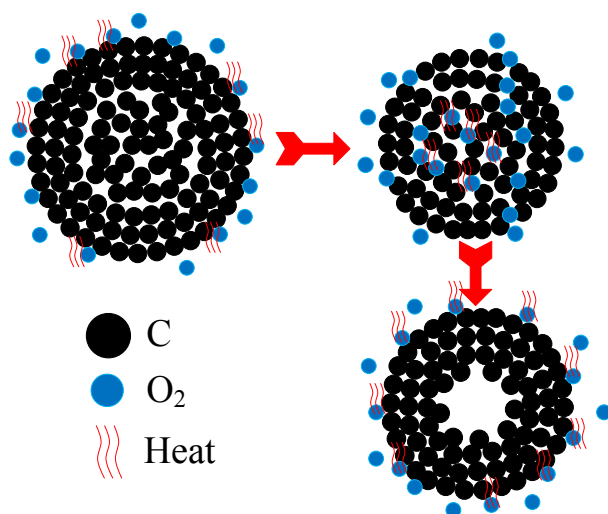


Figure 7 PM model in the oxidation process

Oxidation behaviors, especially for the ignition temperature²⁷, presented closely related to organic compounds. Figure 8 shows the FTIR spectra which detected the functional groups contained in diesel PM. Due to non-vacuum of the FTIR device, two absorption peaks were observed at ~ 3300 cm^{-1} and ~ 2349 cm^{-1} , which were caused by H_2O and CO_2 in the air, respectively. The OC content of raw PM was the highest among the three PM samples, which was agreed with the results in Figure 1. No obvious absorption peak was observed in FTIR spectra for partially oxidized PM, which indicated that OC content almost dropped to zero. After long time aging in air, some OC was adhered to PM surface, which caused ignition temperature drop and low apparent activation energy. In addition, the adhered OC were dominated by low volatile OC, which was demonstrated in Figure 1(b), where the mass loss was almost zero before 400 $^\circ\text{C}$ for aging PM. Although functional groups could be detected using FTIR spectra, Gas Chromatography-Mass Spectrometry (GC-MS)⁵⁴ device was needed to specific OC in future works, further to analyze the adsorption characteristics by PM.

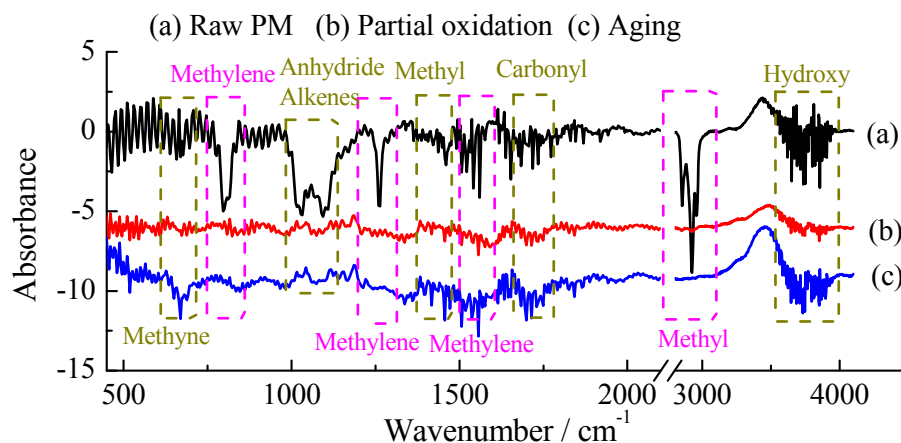


Figure 8 FTIR spectra of different PM samples

Figure 9 shows the Raman spectra of three PM samples. The information of molecular rotation and vibration can be obtained from Raman signals. Raman signals indicated the information of soot disorder and soot graphitization conditions^{40, 55, 56}, which were corresponding to the Raman shifts at $\sim 1380\text{ cm}^{-1}$ and $\sim 1590\text{ cm}^{-1}$, respectively. As shown in the figure, the intensity ratio of G peak to D peak was higher for partially oxidized PM than raw PM and aging PM. Oxidation at high temperature led to higher intensity of G peak, which was caused by the stretching mode of E_{2g} symmetry at sp_2 sites⁵⁷. D peak intensity of partially oxidized PM was partly recovered after aging in air, which resulted from the OC adsorption.

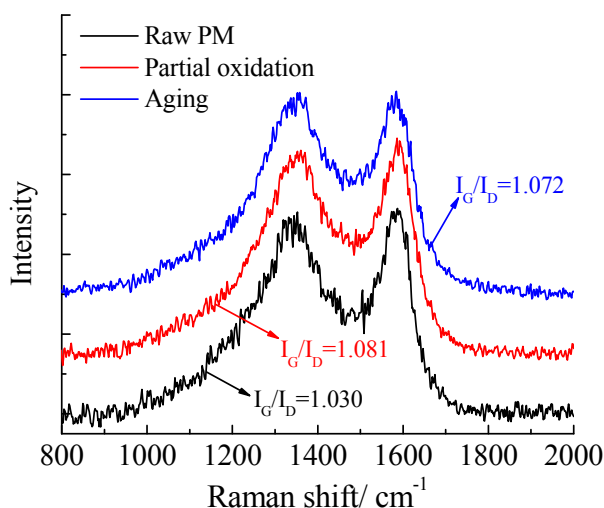


Figure 9 Raman spectra of different PM samples

5. Conclusion

A deep analysis of oxidation behaviors and kinetics was conducted based on three different kinds of PM samples that were raw PM, partially oxidized PM and aging PM. The PM oxidation behavior investigation was performed in different temperature control programs. In addition, the oxidation

1
2
3
4 kinetics were calculated using oxidation profiles and Arrhenius equation. Further, the analysis of
5 nanostructure, FTIR and Raman characteristics were carried out to clarify PM oxidation behaviors.

6
7 The main conclusions were as the following:

8
9 (1) In multi-stage temperature control program, the oxidation profiles presented evident multi-stage
10 reaction process. The isothermal stage of 200 °C had a limited influence on the following process,
11 however, the it was greatly affected by 450 °C and 550 °C isothermal stages. During the isothermal
12 stages of 450 °C and 550 °C, the activation energy increased greatly, and isothermal stages caused
13 the activation energy increase in the following process.

14
15 (2) Heat transfer limitation caused high oxidation rate, with the results of another peak in DTG
16 curves at higher temperature. The activation energy was much lower than normal values due to
17 much heat release when heat transfer limitation happened. Oxidation transferring from the surface
18 into the inner cores caused activation energy to drop in a narrow temperature range; it was also
19 considered as the origin of heat transfer limitation for raw PM.

20
21 (3) The primary diameter decreased evidently after partial oxidation at a high temperature that the
22 peak of primary diameter distribution shifted to smaller diameters. The nanostructure of diesel PM
23 changed from onion like structures to core-shell like structures with void cores. D peak intensity in
24 Raman spectra decreased greatly after partial oxidation, and it was partly recovered after aging in
25 air for a long time.

26 27 28 29 30 31 32 33 34 35 36 37 38 39 40 41 **Acknowledgements**

42 The authors acknowledge School of Chemistry, Beijing Institute of Technology did the experiments.
43 The research described in this paper was supported in part by the EU-funded project optiTruck
44 (grant agreement No 713788) which has the ultimate aimed at developing and test a prototype
45 ‘global fuel optimizer’, capable of achieving a fuel reduction of at least 20% for 40 tonne trucks
46 while still meeting relevant Euro VI emission standards.

47 48 49 50 51 52 53 54 **References**

- 55
56 1. Jiao, P.; Li, Z.; Shen, B.; Zhang, W.; Kong, X.; Jiang, R., Research of DPF regeneration with
57 NO_x-PM coupled chemical reaction. *Appl. Therm. Eng.* **2017**, 110, 737-745.
58
59 2. Matheson, R. <http://news.mit.edu/2017/recycling-air-pollution-make-art-1127>.

3. Gao, J.; Tian, G.; Sornioti, A.; Karci, A. E.; Di Palo, R., Review of thermal management of catalytic converters to decrease engine emissions during cold start and warm up. *Appl. Therm. Eng.* **2019**, *147*, 177-187.
4. R'mili, B.; Boreave, A.; Meme, A.; Vernoux, P.; Leblanc, M.; Noel, L.; Raux, S.; D'Anna, B., Physico-chemical characterization of fine and ultrafine particles emitted during DPF active regeneration of Euro5 Diesel vehicles. *Environ. Sci. Technol.* **2018**, *52*, (5), 3312-3319.
5. Yezerets, A.; Currier, N. W.; Kim, D. H.; Eadler, H. A.; Epling, W. S.; Peden, C. H., Differential kinetic analysis of diesel particulate matter (soot) oxidation by oxygen using a step–response technique. *Applied Catalysis B: Environmental* **2005**, *61*, (1), 120-129.
6. Mühlbauer, W.; Zöllner, C.; Lehmann, S.; Lorenz, S.; Brüggemann, D., Correlations between physicochemical properties of emitted diesel particulate matter and its reactivity. *CoFl* **2016**, *167*, 39-51.
7. López-Fonseca, R.; Landa, I.; Elizundia, U.; Gutiérrez-Ortiz, M.; González-Velasco, J., A kinetic study of the combustion of porous synthetic soot. *Chem. Eng. J.* **2007**, *129*, (1), 41-49.
8. López-Fonseca, R.; Landa, I.; Gutiérrez-Ortiz, M.; González-Velasco, J., Non-isothermal analysis of the kinetics of the combustion of carbonaceous materials. *JTAC* **2005**, *80*, (1), 65-69.
9. Gao, J.; Chen, H.; Chen, J.; Ma, C.; Tian, G.; Li, Y., Explorations on the continuous oxidation kinetics of diesel PM from heavy-duty vehicles using a single ramp rate method. *Fuel* **2019**, *248*, 254-257.
10. Jaramillo, I. C.; Gaddam, C. K.; Vander Wal, R. L.; Lighty, J. S., Effect of nanostructure, oxidative pressure and extent of oxidation on model carbon reactivity. *CoFl* **2015**, *162*, (5), 1848-1856.
11. Gao, J.; Ma, C.; Xing, S.; Sun, L., Oxidation behaviours of particulate matter emitted by a diesel engine equipped with a NTP device. *Appl. Therm. Eng.* **2017**, *119*, 593-602.
12. Ma, C.; Gao, J.; Zhong, L.; Xing, S., Experimental investigation of the oxidation behaviour and thermal kinetics of diesel particulate matter with non-thermal plasma. *Appl. Therm. Eng.* **2016**, *99*, 1110-1118.
13. Gao, J.; Ma, C.; Tian, G.; Chen, J.; Xing, S.; Huang, L., Oxidation activity restoration of diesel particulate matter by aging in air. *Energy Fuels* **2018**, *32*, (2), 2450-2457.
14. Gao, J.; Tian, G.; Ma, C.; Chen, J.; Huang, L., Physicochemical property changes during

- oxidation process for diesel PM sampled at different tailpipe positions. *Fuel* **2018**, 219, 62-68.
15. Gao, J.; Ma, C.; Xing, S.; Sun, L.; Huang, L., A review of fundamental factors affecting diesel PM oxidation behaviors. *Science China Technological Sciences* **2018**, 61, (3), 330–345.
16. Abián, M. a.; Jensen, A. D.; Glarborg, P.; Alzueta, M. U., Soot reactivity in conventional combustion and oxy-fuel combustion environments. *Energy Fuels* **2012**, 26, (8), 5337-5344.
17. Kalogirou, M.; Samaras, Z., Soot oxidation kinetics from TG experiments. *JTAC* **2010**, 99, (3), 1005-1010.
18. Karin, P.; Boonsakda, J.; Siricholathum, K.; Saenkhumvong, E.; Charoenphonphanich, C.; Hanamura, K., Morphology and oxidation kinetics of CI engine's biodiesel particulate matters on cordierite Diesel Particulate Filters using TGA. *International Journal of Automotive Technology* **2017**, 18, (1), 31-40.
19. Shi, Y.; Cai, Y.; Wang, J.; Pu, X.; Linbo, G., Influence of PM size distribution and ingredients on DPF regeneration by non-thermal plasma technology. *PCPP* **2017**, 37, (2), 451-464.
20. Cheng, M.-T.; Chen, H.-J.; Young, L.-H.; Yang, H.-H.; Tsai, Y. I.; Wang, L.-C.; Lu, J.-H.; Chen, C.-B., Carbonaceous composition changes of heavy-duty diesel engine particles in relation to biodiesels, aftertreatments and engine loads. *J. Hazard. Mater.* **2015**, 297, 234-240.
21. Young, L. H.; Liou, Y. J.; Cheng, M. T.; Lu, J. H.; Yang, H. H.; Tsai, Y. I.; Wang, L. C.; Chen, C. B.; Lai, J. S., Effects of biodiesel, engine load and diesel particulate filter on nonvolatile particle number size distributions in heavy-duty diesel engine exhaust. *J. Hazard. Mater.* **2012**, 199, (2), 282-289.
22. Wang, C.; Xu, H.; Herreros, J. M.; Lattimore, T.; Shuai, S., Fuel effect on particulate matter composition and soot oxidation in a direct-injection spark ignition (DISI) engine. *Energy Fuels* **2014**, 28, (3), 2003-2012.
23. Song, J.; Alam, M.; Boehman, A. L.; Kim, U., Examination of the oxidation behavior of biodiesel soot. *CoFl* **2006**, 146, (4), 589-604.
24. Gargiulo, V.; Alfè, M.; Di Blasio, G.; Beatrice, C., Chemico-physical features of soot emitted from a dual-fuel ethanol–diesel system. *Fuel* **2015**, 150, 154-161.
25. Agudelo, J. R.; Álvarez, A.; Armas, O., Impact of crude vegetable oils on the oxidation reactivity and nanostructure of diesel particulate matter. *CoFl* **2014**, 161, (11), 2904-2915.
26. Gao, J.; Ma, C.; Xing, S.; Sun, L.; Huang, L., Nanostructure analysis of particulate matter

- emitted from a diesel engine equipped with a NTP reactor. *Fuel* **2017**, 192, 35-44.
27. Song, J.; Alam, M.; BOEHMAN*, A. L., Impact of alternative fuels on soot properties and DPF regeneration. *CST* **2007**, 179, (9), 1991-2037.
28. Toth, P.; Jacobsson, D.; Ek, M.; Wiinikka, H. J. C., Real-time, in situ, atomic scale observation of soot oxidation. *Carbon* **2019**, 145, 149-160.
29. Sediako, A. D.; Soong, C.; Howe, J. Y.; Kholghy, M. R.; Thomson, M., Real-time observation of soot aggregate oxidation in an Environmental Transmission Electron Microscope. *Proceedings of the Combustion Institute* **2017**, 36, (1), 841-851.
30. Cheng, Y.; Liu, J.; Zhao, Z.; Song, W.; Wei, Y., A new 3DOM Ce-Fe-Ti material for simultaneously catalytic removal of PM and NO_x from diesel engines. *J. Hazard. Mater.* **2018**, 342, 317-325.
31. Ji, Z.; Dai, R.; Zhang, Z., Characterization of fine particulate matter in ambient air by combining TEM and multiple spectroscopic techniques—NMR, FTIR and Raman spectroscopy. *Environmental Science: Processes & Impacts* **2015**, 17, (3), 552-560.
32. Bensaid, S.; Caroca, C.; Russo, N.; Fino, D., Detailed investigation of non-catalytic DPF regeneration. *The Canadian Journal of Chemical Engineering* **2011**, 89, (2), 401-407.
33. Chong, H. S.; Aggarwal, S. K.; Lee, K. O.; Yang, S. Y.; Seong, H., Experimental investigation on the oxidation characteristics of diesel particulates relevant to DPF regeneration. *CST* **2013**, 185, (1), 95-121.
34. Neeft, J. P.; Hoornaert, F.; Makkee, M.; Moulijn, J. A., The effects of heat and mass transfer in thermogravimetric analysis. A case study towards the catalytic oxidation of soot. *Thermochim. Acta* **1996**, 287, (2), 261-278.
35. Bokova, M.; Decarne, C.; Abi-Aad, E.; Pryakhin, A.; Lunin, V.; Aboukais, A., Kinetics of catalytic carbon black oxidation. *Thermochim. Acta* **2005**, 428, (1), 165-171.
36. Gao, J.; Ma, C.; Xing, S.; Zhang, Y.; Liu, J.; Feng, H., Particle-and gas-phase PAHs toxicity equivalency quantity emitted by a non-road diesel engine with non-thermal plasma technology. *Environmental Science and Pollution Research* **2016**, 23, (19), 20017-20026.
37. Yezerets, A.; Currier, N. W.; Kim, D. H.; Eadler, H. A.; Epling, W. S.; Peden, C. H. J. A. C. B. E., Differential kinetic analysis of diesel particulate matter (soot) oxidation by oxygen using a step-response technique. **2005**, 61, (1-2), 120-129.

- 1
2
3
4 38. Sharma, H. N.; Pahalagedara, L.; Joshi, A.; Suib, S. L.; Mhadeshwar, A. B., Experimental
5 study of carbon black and diesel engine soot oxidation kinetics using thermogravimetric analysis.
6
7 *Energy Fuels* **2012**, 26, (9), 5613-5625.
8
9 39. Stanmore, B. R.; Brilhac, J.-F.; Gilot, P., The oxidation of soot: a review of experiments,
10 mechanisms and models. *Carbon* **2001**, 39, (15), 2247-2268.
11
12 40. Gao, J.; Ma, C.; Xia, F.; Xing, S.; Sun, L.; Huang, L., Raman characteristics of PM emitted by
13 a diesel engine equipped with a NTP reactor. *Fuel* **2016**, 185, 289-297.
14
15 41. Qu, L.; Wang, Z.; Zhang, J., Influence of waste cooking oil biodiesel on oxidation reactivity
16 and nanostructure of particulate matter from diesel engine. *Fuel* **2016**, 181, 389-395.
17
18 42. Stratakis, G.; Stamatelos, A., Thermogravimetric analysis of soot emitted by a modern diesel
19 engine run on catalyst-doped fuel. *CoFl* **2003**, 132, (1), 157-169.
20
21 43. Al-Qurashi, K.; Boehman, A. L., Impact of exhaust gas recirculation (EGR) on the oxidative
22 reactivity of diesel engine soot. *CoFl* **2008**, 155, (4), 675-695.
23
24 44. Jaramillo, I. C.; Gaddam, C. K.; Vander Wal, R. L.; Huang, C.-H.; Levinthal, J. D.; Lighty, J.
25 S., Soot oxidation kinetics under pressurized conditions. *CoFl* **2014**, 161, (11), 2951-2965.
26
27 45. Choi, S.; Seong, H., Oxidation characteristics of gasoline direct-injection (GDI) engine soot:
28 Catalytic effects of ash and modified kinetic correlation. *CoFl* **2015**, 162, (6), 2371-2389.
29
30 46. Querini, C. A.; Ulla, M. A.; Requejo, F.; Soria, J.; Sedrán, U. A.; Miró, E. E., Catalytic
31 combustion of diesel soot particles. Activity and characterization of Co/MgO and Co,K/MgO
32 catalysts. *Applied Catalysis B Environmental* **1998**, 15, (1-2), 5-19.
33
34 47. Kleeman, M. J.; Schauer, J. J.; Cass, G. R., Size and composition distribution of fine particulate
35 matter emitted from motor vehicles. *Environ. Sci. Technol.* **2000**, 34, (7), 1132-1142.
36
37 48. Kim, H.; Choi, B., Effect of ethanol–diesel blend fuels on emission and particle size
38 distribution in a common-rail direct injection diesel engine with warm-up catalytic converter.
39
40 *Renewable Energy* **2008**, 33, (10), 2222-2228.
41
42 49. Zervas, E.; Dorlhène, P., Comparison of exhaust particle number measured by EEPS, CPC, and
43 ELPI. *Aerosol Sci. Technol.* **2006**, 40, (11), 977-984.
44
45 50. Rubino, L.; Phillips, P. R.; Twigg, M. V. *Measurements of Ultrafine Particle Number*
46
47 *Emissions from a Light-Duty Diesel Engine Using SMPS, DMS, ELPI and EEPS*; 0148-7191; SAE
48
49 Technical Paper: 2005.
50
51
52
53
54
55
56
57
58
59
60

- 1
2
3
4 51. Wang, S.; Zhu, X.; Somers, L. M. T. In *Effects of EGR at various loads on diesel engine*
5 *performance and exhaust particle size distribution using four blends of RON70 and diesel,*
6 *Sustainable Development of Energy, Water and Environment Systems*, 2016; 2016.
7
8
9 52. Sui, Z.; Zhang, Y.; Peng, Y.; Norris, P.; Cao, Y.; Pan, W.-P., Fine particulate matter emission
10 and size distribution characteristics in an ultra-low emission power plant. *Fuel* **2016**, 185, 863-871.
11
12 53. Wo, H.; Dearn, K. D.; Song, R.; Hu, E.; Xu, Y.; Hu, X., Morphology, composition, and
13 structure of carbon deposits from diesel and biomass oil/diesel blends on a pintle-type fuel injector
14 nozzle. *Tribology International* **2015**, 91, 189-196.
15
16 54. Gao, J.; Ma, C.; Xing, S.; Sun, L.; Liu, J., Polycyclic aromatic hydrocarbon emissions of
17 non-road diesel engine treated with non-thermal plasma technology. *Korean J. Chem. Eng.* **2016**, 33,
18 (12), 3425-3433.
19
20 55. Seong, H. J.; Boehman, A. L., Evaluation of raman parameters using visible raman microscopy
21 for soot oxidative reactivity. *Energy Fuels* **2013**, 27, (3), 1613-1624.
22
23 56. Pawlyta, M.; Rouzaud, J.-N.; Duber, S., Raman microspectroscopy characterization of carbon
24 blacks: spectral analysis and structural information. *Carbon* **2015**, 84, 479-490.
25
26 57. Ferrari, A. C.; Robertson, J., Interpretation of Raman spectra of disordered and amorphous
27 carbon. *PhRvB* **2000**, 61, (20), 14095.
28
29
30
31
32
33
34
35
36
37
38
39
40
41
42
43
44
45
46
47
48
49
50
51
52
53
54
55
56
57
58
59
60